

## Investigation of 2021 wildfire impacts on air quality in southwestern Turkey

Merve Eke <sup>a,b</sup>, Fulya Cingiroglu <sup>c</sup>, Burcak Kaynak <sup>a,\*</sup>

<sup>a</sup> School of Civil Engineering, Department of Environmental Engineering, Istanbul Technical University, Istanbul, Turkey

<sup>b</sup> School of Engineering, Department of Environmental Engineering, Gebze Technical University, Kocaeli, Turkey

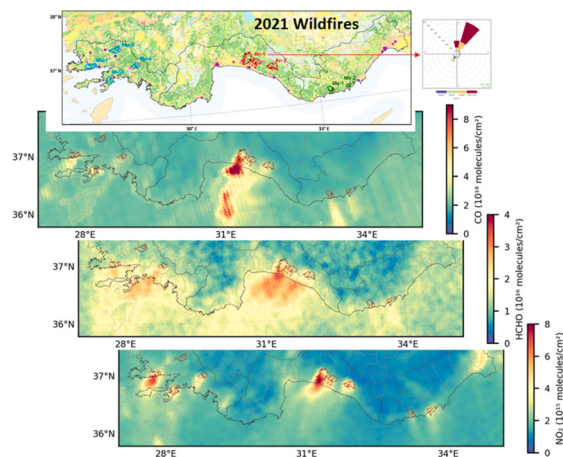
<sup>c</sup> Eurasia Institute of Earth Sciences, Istanbul Technical University, Istanbul, Turkey



### HIGHLIGHTS

- Ground observations were not sufficient to understand the impacts of 2021 wildfires.
- TROPOMI retrievals captured the increase in pollutant levels and pollution transport.
- Transport of fire plumes to the Mediterranean Sea was observed, especially for CO.
- HCHO spatial distribution was different indicating chemical production within fire plume.
- CO and NO<sub>2</sub> showed higher correlations with FRP, and HCHO showed low correlations.

### GRAPHICAL ABSTRACT



### ARTICLE INFO

#### Keywords:

Wildfires  
HCHO  
NO<sub>2</sub>  
CO  
TROPOMI  
Satellite retrievals  
VIIRS  
Fire radiative power

### ABSTRACT

In the summer of 2021, unusually intense wildfires happened in southwestern Turkey, especially in Antalya and Mugla with destroying effects on forests, wildlife, and communities residing there. This study aims to understand the air quality impacts of these wildfires. A time period (June–September 2021) covering pre-, fire, and post-periods was investigated using NO<sub>2</sub> ground-based observations and TROPOMI CO, HCHO, and NO<sub>2</sub> satellite retrievals along with VIIRS FRP. Eight fire regions were selected for detailed analysis in Antalya (An-1-2), Mugla (Mu-1-4), and Mersin (Me-1-2). The highest fire intensity was found in An-1 and followed by Mu-1. CO also showed strongest signals over An-1 ( $6.73 \times 10^{18}$  molecules/cm<sup>2</sup>) with highest levels ( $1.44 \times 10^{19}$  molecules/cm<sup>2</sup>) in the downwind of the wildfires. NO<sub>2</sub> showed fire signals in or in very close proximity to the fire regions with strongest signal and largest impact area in An-1 ( $>8.75 \times 10^{16}$  molecules/cm<sup>2</sup>). HCHO showed a different pattern due to HCHO undergoing chemical production and loss in the wildfire plume. HCHO highest levels were not observed over the fire regions, but inside the transported plume with maximum levels for An-1 ( $3.60 \times 10^{16}$  molecules/cm<sup>2</sup>) and for An-2 ( $3.23 \times 10^{16}$  molecules/cm<sup>2</sup>). CO and NO<sub>2</sub> increase continued not only in fire, but

\* Corresponding author. Department of Environmental Engineering, Istanbul Technical University, Maslak, 34469, Istanbul, Turkey.

E-mail address: [burcak.kaynak@itu.edu.tr](mailto:burcak.kaynak@itu.edu.tr) (B. Kaynak).

also in post-fire period, whereas HCHO levels indicated decreases in post-fire compared to pre-fire period. The increases in column concentrations in fire period ranges from 17.6 to 123.1% for CO, 40.6–116.5% for HCHO and 34.4–294.5% for NO<sub>2</sub>. Higher increases were observed over the Mediterranean Sea especially for CO. Correlations with FRP indicated highest correlations with CO and NO<sub>2</sub> and low correlations with HCHO. This study showed that the capability of sparse, ground-level air quality monitoring stations to capture wildfire impacts are limited in the region, because the plume transport was driven by wind direction and wildfire smoke plumes are elevated due to buoyancy. Satellite retrievals are better for capturing the wildfire plume transport and estimating the overall air quality impacts of wildfires.

## 1. Introduction

Wildfires are essential natural events to sustain ecosystem structure and function. However, there has been an increasing trend in wildfires reported due to climate change in several regions such as Australia, Mediterranean Region, western United States (U.S.), and Canada (Di Virgilio et al., 2019; Keeley and Syphard, 2021; Parente et al., 2018; Richards et al., 2022; Shi et al., 2021; Turco et al., 2014). Wildfires are impacted by meteorological conditions, terrain, land-use change, and population density (Pechony and Shindell, 2010; Jones et al., 2020). Copernicus Atmosphere Monitoring Service (CAMS) reported that warmer and drier weather conditions caused wildfires in central and eastern Mediterranean countries namely Turkey, Greece, Italy, Albania, Algeria, North Macedonia, and Tunisia in the summer of 2021 (CAMS, 2021). It is expected that these conditions will result in increases in the number and magnitude of wildfires in the future (Li et al., 2020).

Wildfires are important sources of particulate matter and gaseous pollutants including greenhouse gases (carbon dioxide (CO<sub>2</sub>), methane (CH<sub>4</sub>), and nitrous oxide (N<sub>2</sub>O)) and air pollutants (carbon monoxide (CO), volatile organic compounds (VOCs), and nitrogen oxides (NO<sub>x</sub>)) (Crutzen et al., 1979; Urbanski et al., 2008). Bondur et al. (2020) demonstrated that annual nitrogen dioxide (NO<sub>2</sub>) emissions caused by wildfires in Russia varied between 0.38 and 1.31 million tons annually for the years 2011–2019. Schneising et al. (2020) detected that Californian wildfires resulted in CO concentration anomalies that reached up to 2.5 mg/m<sup>3</sup> in the boundary layer. Summer wildfires in western Canada during 2001–2019 produced increases of up to 26.5% for CO, 10.5% for NO<sub>2</sub>, and 95.2% for fine particulate matter (PM<sub>2.5</sub>) (Schneider et al., 2021). Wang et al. (2022) indicated a three times-rise in formaldehyde (HCHO) concentration in 2007 and 2008 compared with 2006–2015 period which indicated wildfires in Angeles National Forest in the U.S. Ozone (O<sub>3</sub>) is a secondary pollutant that contributes to radiative forcing (Mickley et al., 2001) and is formed with VOC and NO<sub>x</sub> photochemical reactions (Sillman et al., 1990). Hence, wildfires contribute significantly to O<sub>3</sub> production. O<sub>3</sub> contribution caused by wildfires was predicted as 170 Tg/year that covers 3.5% of total tropospheric O<sub>3</sub> (Jaffe and Wigder, 2012). Wildfire contributions to O<sub>3</sub> production are supported by various monitoring and modeling studies (Cook et al., 2007; Gong et al., 2017; Jaffe et al., 2013; Langford et al., 2023; Lee et al., 2021). On the other hand, recent studies indicated that wildfires may contribute to stratospheric O<sub>3</sub> depletion by affecting chlorine with wildfire aerosols (Lee et al., 2021; McNeill and Thornton, 2023).

Air pollution is one of the major environmental issues that impact human health with 6.67 million premature deaths annually, being the largest contributor to 9 million due to pollution globally every year (Fuller et al., 2022). Wildfires are important sources that affect air quality in short intervals, but produce intense pollution levels compared to other sources (Schneider et al., 2021; Tao et al., 2020). Wildfire smoke exposure affects human health negatively. U.S. Environmental Protection Agency (EPA) stated that wildfire smoke exposure for a few days causes respiratory symptoms and exposure for more than a few days results in a decrease in lung function (EPA, 2022). Studies revealed that short-term exposure results in an increase in hospital admissions with respiratory, cardiovascular, and dermatological complaints

(Fadadu et al., 2021; Reid et al., 2016; Requia et al., 2021). For example, hospital visits rose for dyspnea (48.6–72.6%) and asthma (21.7–40.4%) per day for the 5-day fire period compared to the preceding 20 weekdays during the wildfires in San Diego on October 21–27, 2007 (CDC, 2008). Moreover, wildfire health impact estimations indicated that large fires are related to increased mortality caused by PM<sub>2.5</sub> exposure (Ryan et al., 2021; Tarín-Carrasco et al., 2021). Additionally, recent studies claimed that the risk of COVID-19 and mortality are increased due to wildfire emissions which raise PM, CO, and NO<sub>2</sub> levels during the pandemic (Cortes-Ramirez et al., 2022; Naqvi et al., 2023).

Air pollutants can be monitored with in-situ and/or remote sensing measurements (Aurell et al., 2021; Liao et al., 2021; Yin et al., 2020; Zhao et al., 2022). Considering their semi-random nature, location, and subsequent elevated smoke plumes, it is usually challenging to capture the impacts of wildfires via ground monitoring networks. Research aircraft campaigns are available from time to time (Peng et al., 2021), but they do not have routine air pollutant measurements like ground and satellite remote sensing measurements. Wildfires can be better observed by remote sensing measurements with their global spatial coverage and column concentrations accounting for elevated plumes. With the increase in wildfires, there are studies showing the impacts of wildfire smoke on human health using modeling, ground observations (Aguilera et al., 2021; Chen et al., 2021; Matz et al., 2020) and satellite retrievals (Liu et al., 2015; Xue et al., 2021). However, the lack of surface-level information is the major constraint of satellite retrievals for health applications (Holloway et al., 2021). The TROPOspheric Monitoring Instrument (TROPOMI) is an instrument onboard the Copernicus Sentinel-5P satellite and atmospheric data were available starting from May 2018 (TROPOMI EU, 2023). Ultraviolet (UV), visible (VIS), near-infrared (NIR), and shortwave infrared (SWIR) are in the spectral band of TROPOMI. Thus, CO, HCHO, NO<sub>2</sub>, O<sub>3</sub>, sulfur dioxide (SO<sub>2</sub>), CH<sub>4</sub>, aerosols, and clouds can be monitored (Veefkind et al., 2012). Spatial resolution of the measurements increased up to 3.5 km × 5.5 km at nadir by bringing the along track ground pixel size from 7.0 to 5.5 km since August 2019 for HCHO and NO<sub>2</sub> (Van Geffen et al., 2020). The instrument is also previously used in wildfire research in regional (Alvarado et al., 2020; Griffin et al., 2021) and global studies (Jin et al., 2021; Theys et al., 2020).

Southwestern Turkey was challenged by devastating effects of the 2021 summer wildfires. Forest fires are common in this region during the summer season, and usually have been controlled by the Ministry of Agriculture and Forestry within a short time. However, it took a few weeks to control these intense 2021 summer fires. Fires occurred in Antalya, Mugla, Mersin, Isparta, and Burdur; and the hotspots were in Antalya and Mugla. Wildfires caused a decrease in air quality in these regions. Iban and Sahin (2022) briefly examined the 2021 wildfire impacts on air quality of Mersin and estimated the burned area as 16536 ha. Only spatial distribution was shown for air quality, and concentrations on fire days were given, but there was no quantitative comparison for the fire days. Tariq et al. (2022) investigated the aerosol optical depth (AOD) increase from 0.1 to 2.2 on province level (Antalya and Mugla) during the 2021 Turkey wildfires.

This study aims to focus on the 2021 summer wildfires in southwest Turkey to investigate the impacts on air quality using thermal anomalies data, CO, HCHO, and NO<sub>2</sub> satellite retrievals, ground-based air quality

measurements, and related meteorological parameters. There is not a comprehensive study yet about these unusually intense fire episodes in Turkey which focuses on the specific fire regions that compare pre-fire, fire, and post-fire days with multi-pollutant satellite and ground-based measurements.

## 2. Methodology

Wildfires occur annually in southwestern Turkey during summer periods, but the intensity and duration of the fires were unusual in the summer of 2021 (Global Forest Watch, 2021) (Fig. S1). There was a significant increase in the number of wildfires and their intensity from the end of June until the middle of August 2021 in several regions. The study area covers Antalya, Mugla, and Mersin provinces where significant wildfire anomalies were observed (Fig. 1). These provinces are located on the southwest side of Turkey by the coastline, and mainly covered with mountains. Average summer temperatures are higher than most of the provinces in Turkey and forested areas are a significant portion of the land cover with 1146 (55.6%), 829 (67.5%), 836 (53.5%) thousand hectares in Antalya, Mugla, and Mersin provinces, respectively (MoAF, 2020). Study area was divided into  $1 \times 1 \text{ km}^2$  grids for spatial

calculations.

A four-month period (June–September 2021) was selected as the study period which covers a timeline before and after the wildfire period for the impacted three provinces to observe the temporal variations of the pollutants in pre-fire, fire, and post-fire periods.

The Visible Infrared Imaging Radiometer Suite (VIIRS) sensor of joint NASA/NOAA Suomi National Polar-orbiting Partnership (Suomi NPP) and NOAA-20 satellites ensures 375 m Active Fire Product with one day temporal resolution (Justice et al., 2013). Active fire data includes pixel-integrated Fire Radiative Power (FRP) that provides the magnitude of fires (MW) (Table 1). FRP is a good indicator for the fire intensity. However, it can be drastically underestimated due to cloudiness or thick smoke in some cases (Chow et al., 2022).

2021 VIIRS FRP data was downloaded from NASA FIRMS archive for Turkey (FIRMS, 2022). FRP was used to assess seasonal fire intensity by years, observe a temporal change of fires for the selected four months, and determine the fire intensity for the study interval. The daily, monthly, and selected fire period FRP were calculated for  $1 \times 1 \text{ km}^2$  gridded study domain using ArcGIS, and spatial distribution was determined. According to hotspots, fire regions (FR) were selected. Two strong signal regions were observed over Antalya and Mersin each, and

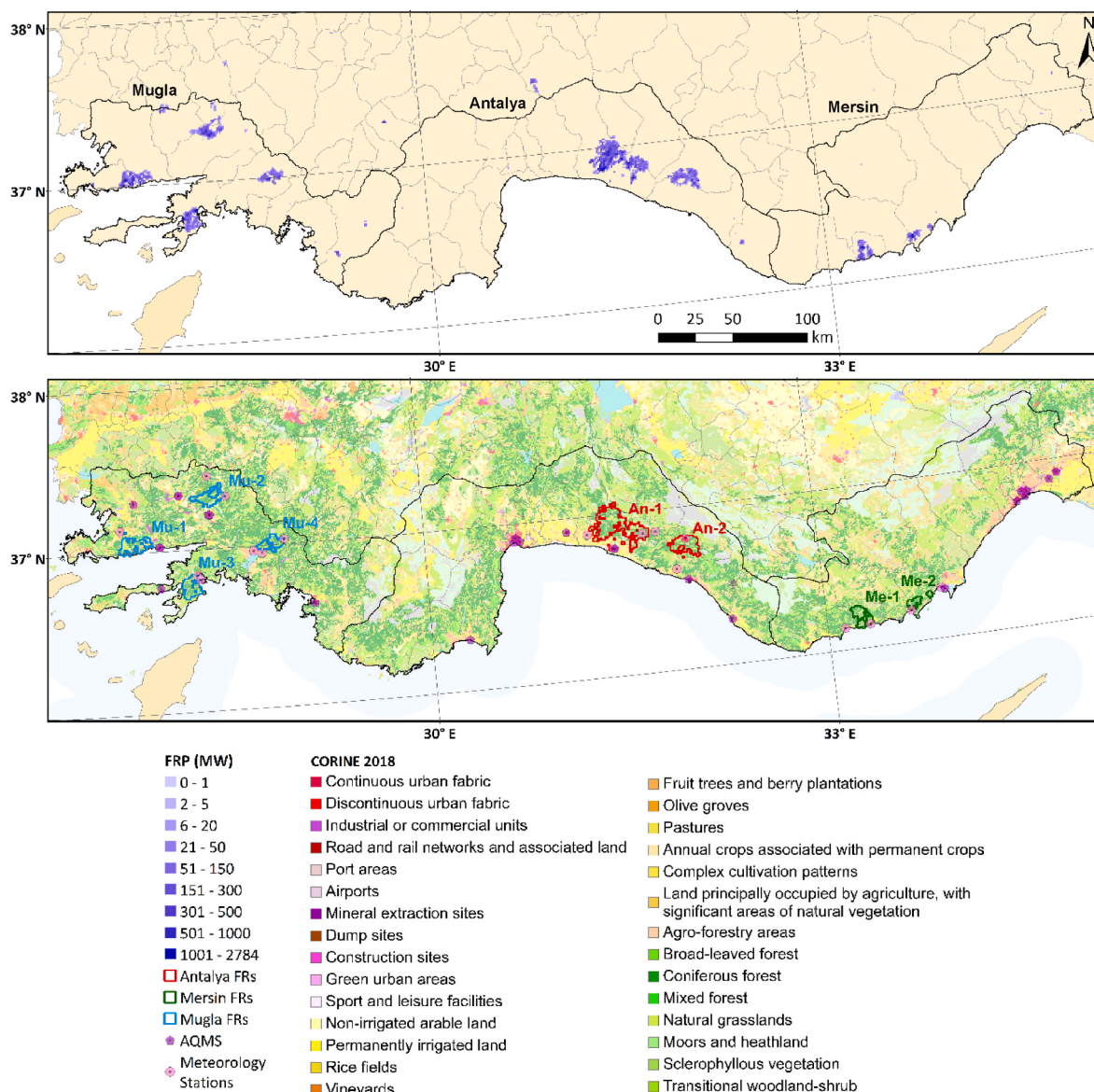


Fig. 1. Spatial distribution of FRP and the study area with FRs.

**Table 1**

The fire region information along with air quality monitoring and meteorology stations.

Fire			Air Quality				Meteorology	
Region (FR)	Districts	Fire Intervals	Station Name	Distance to FR – Direction	Measured Pollutants	Data Availability	Station ID	Distance to AQMS
An-1	Manavgat, Akseki, Ibradi	Jul 28 – Aug 6	Manavgat	10 km – S	NO <sub>2</sub>	84%	18839*	22 km
					PM <sub>10</sub>	100%	17917	21.5 km
					O <sub>3</sub>	100%	17954	0 km
An-2	Alanya, Gundomus	Jul 29 – Aug 13	Alanya	19 km – S	NO <sub>2</sub>	84%	18012*	28.5 km
					PM <sub>10</sub>	100%	19154	10.5 km
Me-1	Aydincik	Jul 15–17 Jul 29–31					18061*	
Me-2	Silifke	Jul 29–31	Tasucu	16 km – E	NO <sub>2</sub>	53%	18284	
					PM <sub>10</sub>	0%	18870*	27.5 km
					O <sub>3</sub>	55%	17479	2.5 km
					SO <sub>2</sub>	70%		
					NO <sub>2</sub>	43%		
Mu-1	Bodrum, Milas	Aug 1–7	Milas	25 km – N	PM <sub>10</sub>	44%	17293	
					O <sub>3</sub>	46%		
					SO <sub>2</sub>	46%		
			Milas Oren	6 km – E	NO <sub>2</sub>	40%		
					PM <sub>10</sub>	34%	17921*	0 km
Mu-2	Mentese, Kavaklıdere, Yatağan	Aug 4–7	Musluhittin	6.5 km – S	PM <sub>2.5</sub>	38%		
					O <sub>3</sub>	48%		
					SO <sub>2</sub>	52%		
			Trafik	6.5 km – S	PM <sub>10</sub>	100%	18629*	17 km
					SO <sub>2</sub>	99%	18022	27 km
Mu-3	Marmaris	Jul 29 – Aug 5	Datca	15 km – W	NO <sub>2</sub>	36%	17886	
					PM <sub>10</sub>	34%	17292	26 km
					PM <sub>2.5</sub>	36%	0 km	
Mu-4	Koycegiz	Jul 29 – Aug 12	Fethiye	47 km – SE **	CO	35%		
					NO <sub>2</sub>	42%	18019	50 km
					PM <sub>10</sub>	38%	18627	49 km
					CO	42%	17924*	55 km

\*Indicates the closest meteorology stations to fire regions.

\*\*Not included in the assessment due to the distance to the fire region.

four for Mugla (Fig. 1). High signals with limited areas were not taken into consideration as FRs. Eight FRs were selected in the study area; two regions in Antalya as An-1, An-2, four regions in Mugla as Mu-1, Mu-2, Mu-3, Mu-4, and two regions in Mersin as Me-1, and Me-2 (Fig. 1). Daily total FRP was calculated for these eight FRs to understand daily changes in fire intensities and compare them with pollution levels. 28 July–7 August period was selected as the overall fire episode, and the change in pollution levels in this episode was compared with pre-fire and post-fire periods. Additionally, fire days (FD) were selected separately for every FR based on FRP  $\geq 10$  MW; other days were assigned as non-fire days (NFD).

Air quality of the region was assessed with satellite retrievals and ground-based observations. There are currently 23 air quality monitoring stations (AQMS) in the national network of the Ministry of Environment, Urbanization, and Climate Change (MoEUCC) monitoring hourly levels of CO, NO<sub>2</sub>, O<sub>3</sub>, SO<sub>2</sub>, and PM (PM<sub>2.5</sub>, PM<sub>10</sub>) for the study area (MoEUCC, 2022) (Table 1) (Fig. 1). Seven AQMS were selected according to proximity to the fire regions; Manavgat and Alanya in Antalya, Milas, Milas-Oren, Musluhittin, and Trafik in Mugla, and Tasucu in Mersin provinces. Manavgat, Alanya, and Tasucu AQMSs provided NO<sub>2</sub> measurements with 84%, 84%, and 53% data availability for the study period. However, Milas, Milas-Oren, and Trafik AQMSs did not have measurements prior to Aug 6. Additionally, Musluhittin AQMS did not include NO<sub>2</sub> and CO measurements. Hence, these stations were not used because they are not representative in terms of selected period and/or pollutants. Manavgat, and Tasucu AQMSs had NO<sub>2</sub> and O<sub>3</sub>. Alanya AQMS had only NO<sub>2</sub> measurements, and daily averages were calculated for these AQMSs.

TROPOMI CO, HCHO, and NO<sub>2</sub> retrievals between Jun 1–Sept 30

were obtained from the NASA Goddard Earth Sciences Data and Information Services Center (GES-DISC) (GES, 2023) (Table S1). Datasets were filtered according to data quality criteria given in data documentation (qa>0.5 for CO, HCHO, and NO<sub>2</sub>). Satellite retrievals for all pollutants were examined in three ways. Firstly, they were spatially matched and average column concentrations were calculated for 1 × 1 km<sup>2</sup> gridded domain to observe the spatial distribution of the pollutants in the study region. Secondly, daily average column concentrations within 3 km around eight FRs were estimated to understand the changes in pollution levels in FRs. A similar method was applied around AQMSs, daily average column concentrations within 6 km around AQMSs were estimated to understand whether the AQMSs were affected, since ground-based observations were limited in terms of pollutant type and temporal coverage during the study period (Table 1).

Meteorological conditions are important in terms of fire intensity, dispersion, and chemistry of the pollutants. There are 21 meteorology stations close to fire regions (Fig. 1) and ten of them were selected to investigate the meteorological impacts (Table 1). 2021 meteorological data was taken from the Turkish State Meteorological Service (TSMS) (TSMS, 2022). July–September 2021 hourly wind speed, wind direction, temperature, and radiation data were investigated. Daily averages were calculated for wind speed, temperature, and radiation. Wind and pollution roses were created for different periods to understand the source of pollution levels in AQMS locations.

After processing the datasets, June–September 2021 time series of FRP, pollutant concentrations, wind speed, and temperature were created for eight selected fire regions. Time series of pollutant retrievals were created by calculating daily average column concentrations for each FRs. Moreover, correlation between FRP and pollution levels were

investigated. Average pollution levels for pre-fire (Jun 1-Jul 27), fire (Jul 28-Aug 7), and post-fire (Aug 8-Sep 30) periods were calculated and compared. Change in concentrations of fire and post-fire periods from pre-fire period were calculated (Equations (1) and (2)). Similarly, FD and NFD pollution levels and changes were calculated and compared

(Table S1).

$$\Delta Fire (\%) = \frac{Fire - (Prefire)}{Prefire} \times 100 \quad (1)$$



**Fig. 2.** Time series of daily FRP, CO, HCHO, and NO<sub>2</sub> column concentrations, and NO<sub>2</sub> and O<sub>3</sub> ground measurements for all FRs.

$$\Delta\text{Postfire} (\%) = \frac{(\text{Postfire}) - (\text{Prefire})}{\text{Prefire}} \times 100 \quad (2)$$

For the spatial comparison, pollution distribution maps of pre-fire, fire, and post-fire periods were prepared. Pre-fire period with no significant fires in the region can be taken as background pollution, because the pollution levels in fire regions were not yet affected by fires. Thus, differences of fire and post-fire averages to pre-fire average were estimated to investigate the increases in pollution levels due to wildfires of 2021.

### 3. Results and discussion

FRP changes for all FRs were examined with time series analysis for the summer of 2021 (June–September). Results showed that fires occurred between mid-July and mid-August. Although fires were observed on Jul 10 in Mu-1, and Jul 15 in Me-1, the most intense fires for all regions started on Jul 28 (Fig. 2). The maximum daily total FRP was observed in An-1 with 29218 MW, followed by Mu-1 with 11684 MW and Mu-3 with 9010 MW. In Mu-4, fire intensity was significantly lower than in other regions with a daily maximum FRP of 2633 MW. FRP significantly decreased after Aug 7 for all regions and last fires of Mu-4 ended on Aug 10. Temporal changes of CO, HCHO, and NO<sub>2</sub> column concentrations over all FRs were also investigated (Fig. 2). CO column concentrations were usually below  $2 \times 10^{18}$  molecules/cm<sup>2</sup> for all regions before the fires started. CO column concentration increased more than three times on Jul 29 up to  $6.73 \times 10^{18}$  molecules/cm<sup>2</sup> in An-1. Additionally, although decreased after the fires, CO levels were relatively higher until the end of August when compared with the pre-fire period. The highest CO peaks were observed for An-1 and Mu-1, but peak CO levels in all FRs reached over  $5.0 \times 10^{18}$  molecules/cm<sup>2</sup>. Me-1 showed two smaller peaks on Jul 15–16, and Jul 29–30 which matched with the fire intervals of the region (Table 1). The limited available NO<sub>2</sub> and O<sub>3</sub> AQMS measurements indicated NO<sub>2</sub> peaks in Alanya (An-1) and in Manavgat (An-2) and O<sub>3</sub> enhancements at the end of the fire interval until Aug 15 in Manavgat (An-2) suggesting ozone formation after the fires (Fig. 2). CO column concentrations were usually below  $2 \times 10^{18}$  molecules/cm<sup>2</sup> in the pre-fire period but higher in post-fire until end of the August for all FRs (Fig. 3). HCHO levels showed more variation and indicate two peaks in the FRs, especially in Mugla prior to the fire period. In addition, a sharp decrease was observed around July 4–8. The highest HCHO levels were usually seen in Mugla FRs (Mu-1 and Mu-4). There were increases in HCHO column concentrations up to  $3.3 \times 10^{16}$  molecules/cm<sup>2</sup> from Jul 28 to Aug 5 peaking on Aug 4–5 in all FRs except Me-1 and Me-2. In addition, Jul 15–17 fire interval could not be observed due to limited data availability. After fire period ended, HCHO levels did not show an increase (relative to the pre-fire period) like the CO and NO<sub>2</sub> levels. NO<sub>2</sub> column concentrations showed similar trends with CO with lower levels in the pre-fire period. Higher levels up to  $3 \times 10^{15}$  molecules/cm<sup>2</sup> were observed at times which were possibly associated with coal-fired power plants around Mu-1 region. The first NO<sub>2</sub> fire peak was observed in Me-1 with  $4.2 \times 10^{15}$  molecules/cm<sup>2</sup> on Jul 15 and then NO<sub>2</sub> column concentration increased up to  $1.0 \times 10^{16}$  molecules/cm<sup>2</sup> in Mu-3. The NO<sub>2</sub> peaks indicated 4–8 times increase compared with pre-fire averages. Similar to HCHO, NO<sub>2</sub> pollution levels went back to usual pollution level after fires except Mugla regions. AQMS NO<sub>2</sub> measurements for An-1, An-2, and Me-2 were examined with available data. NO<sub>2</sub> concentrations showed a sharp increase after Jul 28 in An-1 region (Alanya and Manavgat AQMSs). NO<sub>2</sub> concentration reached  $63.8 \mu\text{g}/\text{m}^3$  on Jul 31. Wind roses for the selected fire period (Jul 28–Aug 7) showed the dominant winds from north for An-1 and northeast for An-2 which explains the transport of fire plumes to the AQMSs (Fig. S2). A significant increase in NO<sub>2</sub> was observed during the fire period for An-1 with higher than  $60 \mu\text{g}/\text{m}^3$ . NO<sub>2</sub> concentrations for Me-2 (Tasucu AQMS) were limited and did not show an increase similar to An-1 and An-2 during the fire period. The wind rose of Me-2 AQMS

showed varying wind directions and the impacts of fires were not observed in this station. The daily CO, HCHO, and NO<sub>2</sub> column concentrations over the AQMSs also indicated limited capture of wildfire pollution, mainly in Manavgat, Alanya, and Milas Oren (Fig. S3). Ground level NO<sub>2</sub> concentration measurements at AQMSs indicated increases in An-1 and An-2, but decreases in Me-2 on FDs compared to NFDs. Tasucu AQMS is located on the east of Me-2 fire region, hence cannot capture the fire impacts (Table 1). These findings indicated that capturing the impacts of these fires could not be possible even if there is sufficient data at the AQMSs.

CO, HCHO, and NO<sub>2</sub> column concentrations in pre-fire, fire, and post-fire periods were compared to understand the air quality within the region and changes during the fire period for all FRs. Daily average column concentrations over FRs were used to prepare boxplots. Although there is a wide range in the column concentrations in fire periods, median values were significantly higher than pre-fire concentrations for all pollutants (Fig. 3). Average column concentrations for periods showed the highest increase in NO<sub>2</sub> in pollutants and An-1 in regions (Table 2). When post-fire concentrations were compared with pre-fire concentrations, CO and NO<sub>2</sub> showed higher levels, and HCHO showed lower levels. Post-fire CO levels were 12.3–18.6% and NO<sub>2</sub> levels were 0.7–37.7% higher than pre-fire levels. CO and NO<sub>2</sub> are mainly associated with combustion during the fires in those remote forested regions, however, HCHO can also come from oxidation of VOCs from biogenic emissions in the region. After the fires, a decrease in the biogenic emissions was expected because of the fire damage which can explain the minor decreases (0.1–14.5%) in HCHO concentrations except Mu-2 indicating a 12.6% increase (Table 2).

Me-1 and Me-2 fire intensities were less than other regions except Mu-4, and have shortest fire intervals within FRs. In addition, a high FRP signal indicating a fire in Me-1 was observed on July 15–16 which was not within the overall fire period. Thus, in addition to period selection, daily selection was performed as FD and NFD for each region. This analysis also supported pollutant concentration increases on fire day averages and showed higher differences for Me-1 and Me-2 FRs (Table S1, Fig. S4).

The pollutants can be transported away from the fire regions, thus spatial distributions of CO, HCHO, and NO<sub>2</sub> column concentrations were examined for a wider region covering all FRs in pre-fire, fire, and post-fire period. Strong signals of pollutants were observed in and nearby the fire regions during the fire period (Fig. 4). The strongest and largest signals farther transported from the region were observed for CO in An-1 that reaches  $1.44 \times 10^{19}$  molecules/cm<sup>2</sup> to the south-southwest direction approximately 15 km away to the Mediterranean Sea. A more distant plume was also observable around 80–110 km away from the region with significant CO levels. Transport to southwest was observed in An-2 with lower column concentrations. In Mugla province, strongest CO signals were observed in Mu-1 with column concentrations reaching up to  $6.29 \times 10^{18}$  molecules/cm<sup>2</sup> in the south-southwest direction followed by Mu-3. Mu-2 showed lowest levels column concentrations ( $2.00$ – $2.85 \times 10^{18}$  molecules/cm<sup>2</sup>) which can be explained by the fires continuing for four days in that region (Table 1) and wind direction was highly variable (Fig. S3). In both regions in Mersin, transport to south-southeast direction was observed, but a dispersion to the north was also seen, unlike other regions in Me-2. The levels in Me-1 were higher and farther transported up to 85 km reaching Cyprus. The previous validation results of TROPOMI CO against ground-based data sets showed low systematic difference ( $6.5 \pm 3.54\%$ ) and high correlation (above 0.9) indicating this high-quality data has acceptable systematic and random uncertainties (Sha et al., 2021).

HCHO signals and spatial distribution showed a different pattern. It is expected considering the short lifetime of HCHO compared to CO, and increasing HCHO with the physical age of the wildfire plumes due to a balance between chemical production and loss (Liao et al., 2021). The highest levels were not observed over the fire regions, but within the transported plume, with maximum column concentrations within 10 km

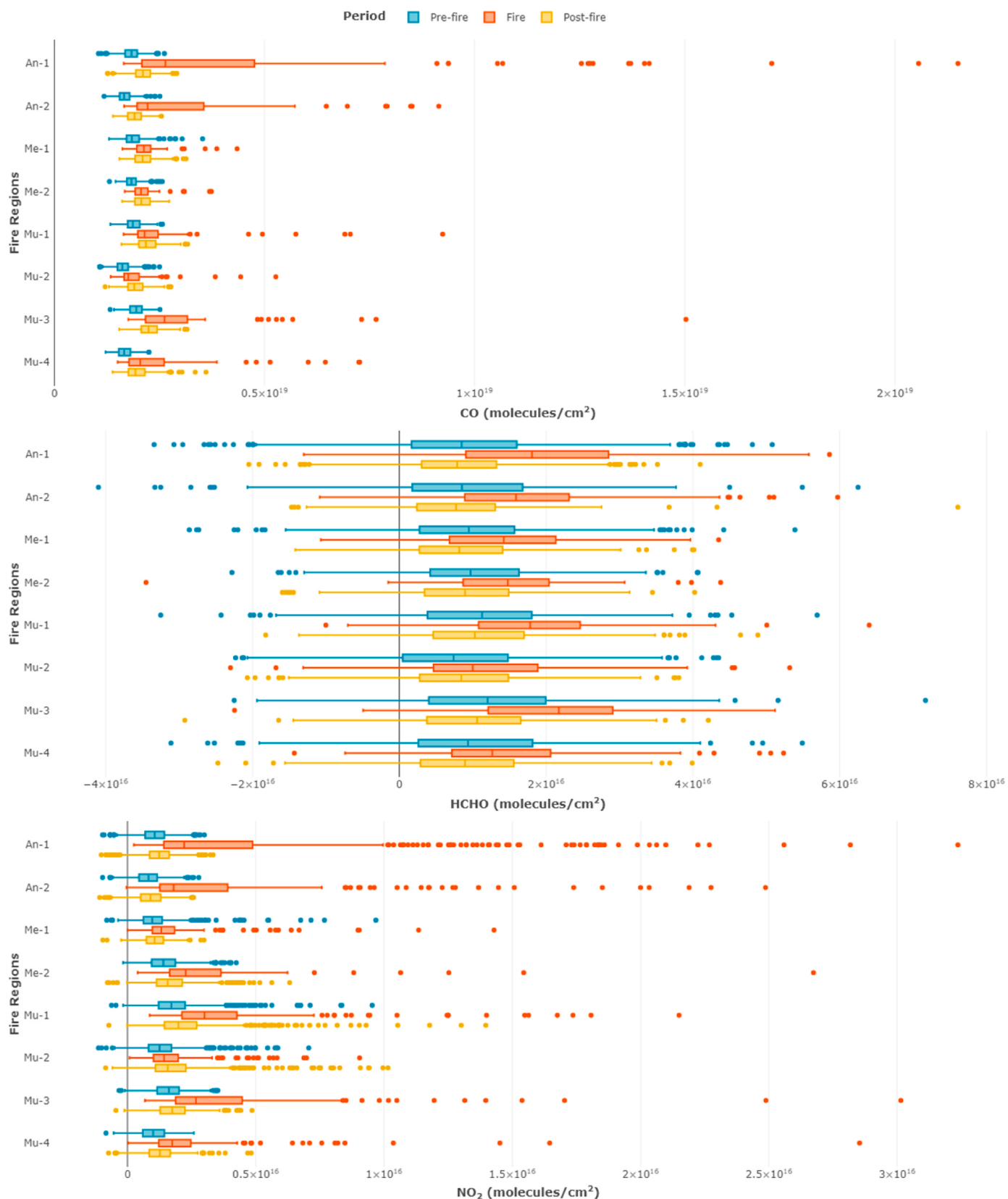


**Fig. 3.** Comparison of pre-fire, fire, post-fire CO, HCHO, and NO<sub>2</sub> (from top to bottom) column concentrations for all FRs.

**Table 2**

CO, HCHO, and NO<sub>2</sub> average column concentrations for FRs in pre-fire, fire, and post-fire intervals and percent changes ( $\Delta$ ) of fire and post-fire compared to pre-fire period.

Pollutants	Interval	An-1	An-2	Me-1	Me-2	Mu-1	Mu-2	Mu-3	Mu-4
CO (molecules/cm <sup>2</sup> )	Pre-fire	1.83E+18	1.68E+18	1.89E+18	1.85E+18	1.89E+18	1.64E+18	1.95E+18	1.68E+18
	Fire	4.08E+18	3.08E+18	2.23E+18	2.18E+18	2.61E+18	1.99E+18	3.28E+18	2.63E+18
	Post-fire	2.12E+18	1.92E+18	2.12E+18	2.10E+18	2.22E+18	1.94E+18	2.27E+18	1.99E+18
	$\Delta$ (Fire)	<b>123.1%</b>	<b>83.1%</b>	<b>18.3%</b>	<b>17.6%</b>	<b>37.8%</b>	<b>21.5%</b>	<b>68.4%</b>	<b>57.0%</b>
	$\Delta$ (Postfire)	15.9%	14.0%	12.3%	13.4%	17.6%	18.4%	16.7%	18.6%
HCHO (molecules/cm <sup>2</sup> )	Pre-fire	8.96E+15	8.74E+15	9.33E+15	1.02E+16	1.08E+16	7.90E+15	1.21E+16	1.04E+16
	Fire	1.94E+16	1.72E+16	1.42E+16	1.48E+16	1.80E+16	1.18E+16	2.11E+16	1.46E+16
	Post-fire	8.29E+15	7.74E+15	8.60E+15	9.15E+15	1.08E+16	8.90E+15	1.03E+16	9.21E+15
	$\Delta$ (Fire)	<b>116.5%</b>	<b>96.8%</b>	<b>51.8%</b>	<b>44.9%</b>	<b>66.1%</b>	<b>49.9%</b>	<b>75.0%</b>	<b>40.6%</b>
	$\Delta$ (Postfire)	-7.5%	-11.5%	-7.9%	-10.3%	-0.1%	12.6%	-14.5%	-11.2%
NO <sub>2</sub> (molecules/cm <sup>2</sup> )	Pre-fire	1.07E+15	8.25E+14	1.06E+15	1.48E+15	1.82E+15	1.35E+15	1.60E+15	9.98E+14
	Fire	4.22E+15	3.61E+15	1.89E+15	3.18E+15	3.89E+15	1.81E+15	4.00E+15	2.63E+15
	Post-fire	1.24E+15	9.10E+14	1.07E+15	1.71E+15	2.23E+15	1.85E+15	1.80E+15	1.27E+15
	$\Delta$ (Fire)	<b>294.5%</b>	<b>336.9%</b>	<b>77.9%</b>	<b>115.9%</b>	<b>113.6%</b>	<b>34.4%</b>	<b>150.1%</b>	<b>163.1%</b>
	$\Delta$ (Postfire)	15.9%	10.3%	0.7%	15.8%	22.5%	37.7%	12.6%	26.9%

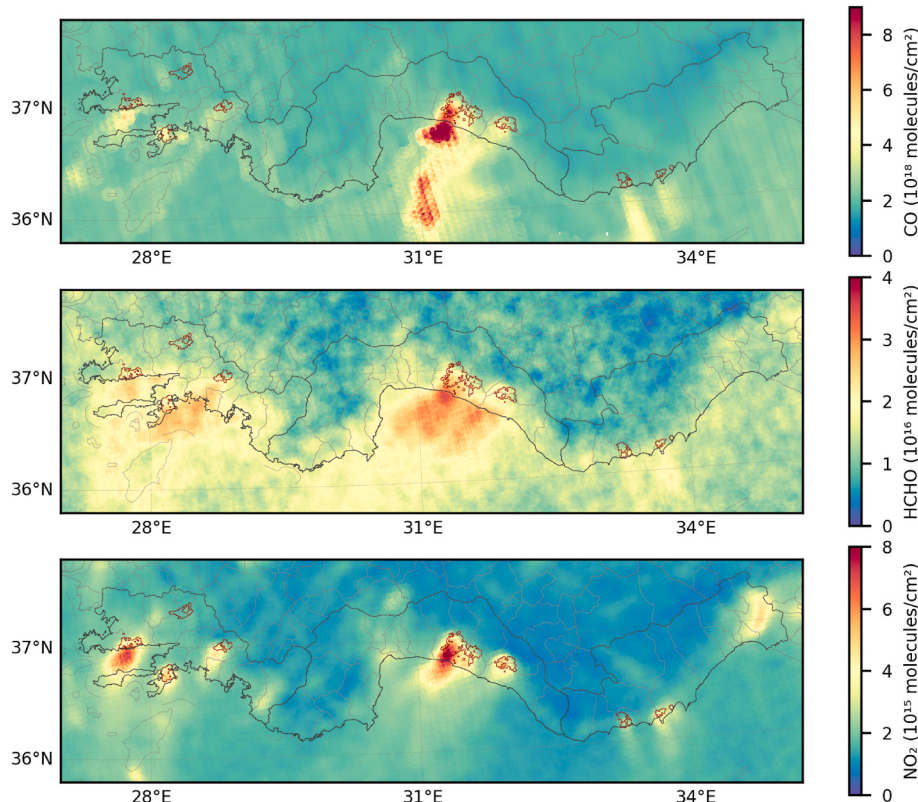


**Fig. 4.** Spatial distribution of CO, HCHO, and NO<sub>2</sub> (from top to bottom) average column concentrations for the fire period with fire regions delineated in red.

of An-1 ( $3.60 \times 10^{16}$  molecules/cm<sup>2</sup>) and 30 km of An-2 ( $3.23 \times 10^{16}$  molecules/cm<sup>2</sup>). For other regions, similar findings were observed. One significant difference from CO levels was that HCHO levels transported from Mu-4 and Mu-3 were significantly higher with a larger impacted region (Fig. 4). These results indicated secondary HCHO formation from the VOCs formed during the fires. Validation with MAX-DOAS measurements showed TROPOMI HCHO data are systematically low for elevated levels (HCHO columns larger than  $8 \times 10^{15}$  molecules/cm<sup>2</sup>) (De Smedt et al., 2021) similar with the FTIR validation (Vigouroux et al., 2020). These results indicate there could be underestimations for HCHO for the wildfire plumes, because average HCHO levels are well above the mentioned level (Fig. 4).

TROPOMI has an outstanding ability to detect tropospheric NO<sub>2</sub> on a very high horizontal resolution and NO<sub>2</sub> vertical column densities are highly correlated with the aircraft and surface in-situ observations, and

the ground-based remote-sensing measurements with a low bias (15–30 %) (Griffin et al., 2019). NO<sub>2</sub> with shorter lifetime and better retrievals, showed fire signals in or in very close proximity to the fire regions. Similar to CO and HCHO, strongest signal with largest impact area was in An-1 with levels exceeding  $8.75 \times 10^{16}$  molecules/cm<sup>2</sup> with high levels over  $6.00 \times 10^{16}$  molecules/cm<sup>2</sup> within 15 km of the region, followed by Mu-1. The relative pollution magnitudes and transport were similar with CO levels within the close proximity to fire regions. An-2, Mu-3, and Mu-4 showed smaller impacted areas and NO<sub>2</sub> levels in Me-1 showed the lowest signal with below  $3 \times 10^{15}$  molecules/cm<sup>2</sup> due to the reasons explained for CO concentrations. Although Mu-2 FRP signals were stronger than Mu-4, Me-1, and Me-2, strong pollution signals were not observed in this region. Calmer winds with varying wind direction may impact the intensity of the wildfires and pollution levels. The wildfire plumes were transported mainly to the south towards the

Mediterranean Sea with high levels of CO and HCHO. Although CO signals were stronger in spatial distributions, changes over the FRs were lower compared to NO<sub>2</sub>. The changes in fire period compared to pre-fire period were calculated for a wider region covering all FRs and showed significantly higher enhancements in the transported regions, especially over the Mediterranean Sea (Fig. 5). An-1 and An-2 plumes caused CO enhancements in a large area with increases up to 500%. Mu-1 and Me-2 were the other two regions with significant increases towards the south. HCHO signals were more widespread with lower enhancements, and NO<sub>2</sub> enhancements were intense and close to the fire regions. Lowest enhancements were observed in Mu-2, similar to previous findings. Percent changes of post-fire CO, HCHO, and NO<sub>2</sub> column concentrations to pre-fire indicated consistent enhancements after the fires except HCHO for the wider region similar to FRs (Fig. S5).

Our findings are very similar to Jin et al. (2023) showing NO<sub>2</sub> enhancement concentrated near the regions actively burning, whereas HCHO enhancement is far-reaching, extending from the source regions to downwind due to the secondary production of HCHO from longer-lived VOCs such as ethene. A recent ozone sensitivity study also indicated that chemical reactivity of VOCs affects downwind of the fire regions (Pouyaei et al., 2023).

The relationships of the pollutants with each other and with FRP were investigated for understanding the formation of these pollutants in the FRs. Correlations between daily FRP and CO, HCHO, and NO<sub>2</sub> column concentrations were calculated for individually and for all FRs together. Highest overall correlation with FRP was found for CO ( $R = 0.60$ ) with highest FR correlations of An-2 ( $R = 0.88$ ) and Mu-3 ( $R = 0.84$ ), and lowest for Me-2 ( $R = 0.21$ ) (Fig. 6). NO<sub>2</sub> showed an overall correlation of  $R = 0.50$  with highest FR correlations of An-2 ( $R = 0.85$ ) and Mu-3 ( $R = 0.85$ ), and lowest for Mu-1 ( $R = 0.47$ ). HCHO, on the other hand, has low overall and FR correlations, usually with low statistical significance. The slopes of the correlation plots with FRP were significantly different for FRs with similarities for the pollutants in the same FR indicating different formation rates in FRs. The overall correlation between CO and NO<sub>2</sub> was the highest with An-1 ( $R = 0.92$ ), An-2

( $R = 0.86$ ), and Mu-3 ( $R = 0.82$ ) indicating the impact of fires. However, similar to spatial distributions, HCHO correlations with CO and NO<sub>2</sub> were low indicating a different formation mechanism and temporal changes for HCHO. These results indicating higher correlations in CO and NO<sub>2</sub> and lower in HCHO are consistent with the formation time of these pollutants in wildfires. Although highest FRP peak was observed in Mu-1, correlations were lower for all pollutants compared with other Mugla regions. A further investigation on correlations with respect to fire days revealed correlations were higher when fire days were selected for FRs (Fig. S6).

FRP as an indicator of the fire-generated pollutants includes uncertainties, since FRP shows two snapshots in a day (at 13:30 and 1:30 in this study with VIIRS S-NPP) and has limitations under cloudy or thick smoke conditions. Hence, increased pollution level that caused by wildfires can be underestimated in some cases (Chow et al., 2022). Geostationary instrument products can provide more accurate results with better temporal resolution (Yin et al., 2019), which is not available in the study region. Although FRP may not reflect all fires that continued for several days, significant correlations were observed.

#### 4. Conclusions

The study showed that 2021 summer fires impacted air quality negatively in southwestern Turkey with increases in CO, HCHO, and NO<sub>2</sub> concentrations during the fire period. Most intense fires were observed in An-1 with the highest FRP and largest fire area. Meteorological conditions for An-1 showed that wind speed peaked at the same time as FRP, indicating the impact of wind on fire intensity, and temperatures were relatively higher. Consequently, strongest pollutant signals were observed in An-1 for all pollutants. Time series showed a sharp increase after fires started, and column concentrations peaked compared with pre-fire and post-fire levels. CO, HCHO, and NO<sub>2</sub> concentrations increased the most in An-1 FR with 123.1%, 116.5%, and 294.5% in the fire period, respectively. Additionally, highest increases were observed for NO<sub>2</sub> for all FRs except Mu-2. Spatial distribution

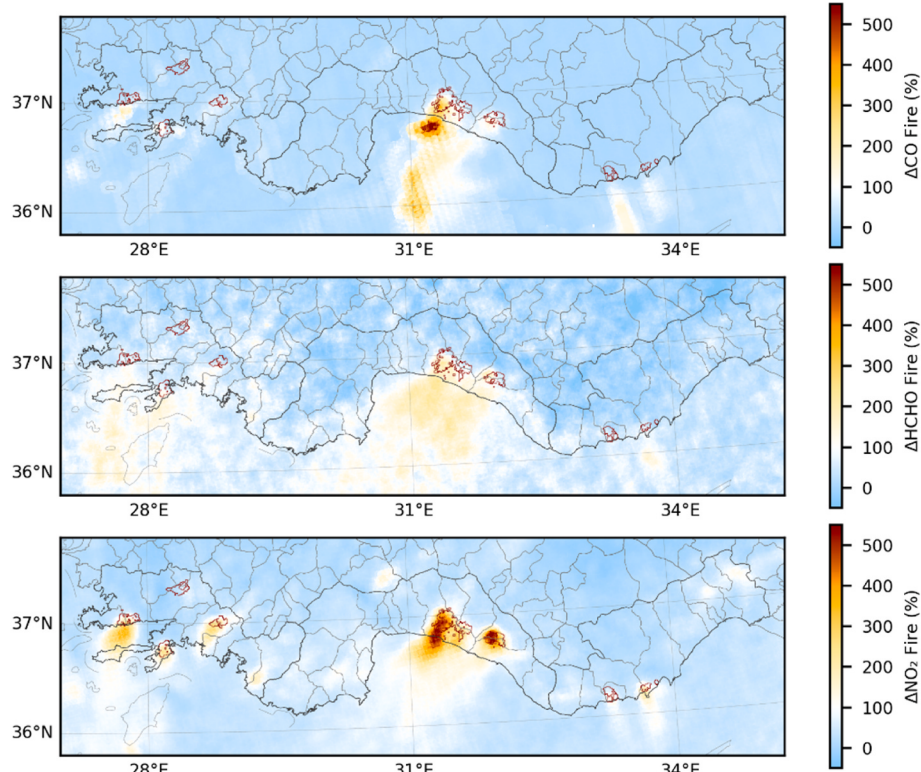


**Fig. 5.** Percent change of fire to pre-fire period CO, HCHO, and NO<sub>2</sub> (from top to bottom) average column concentrations.

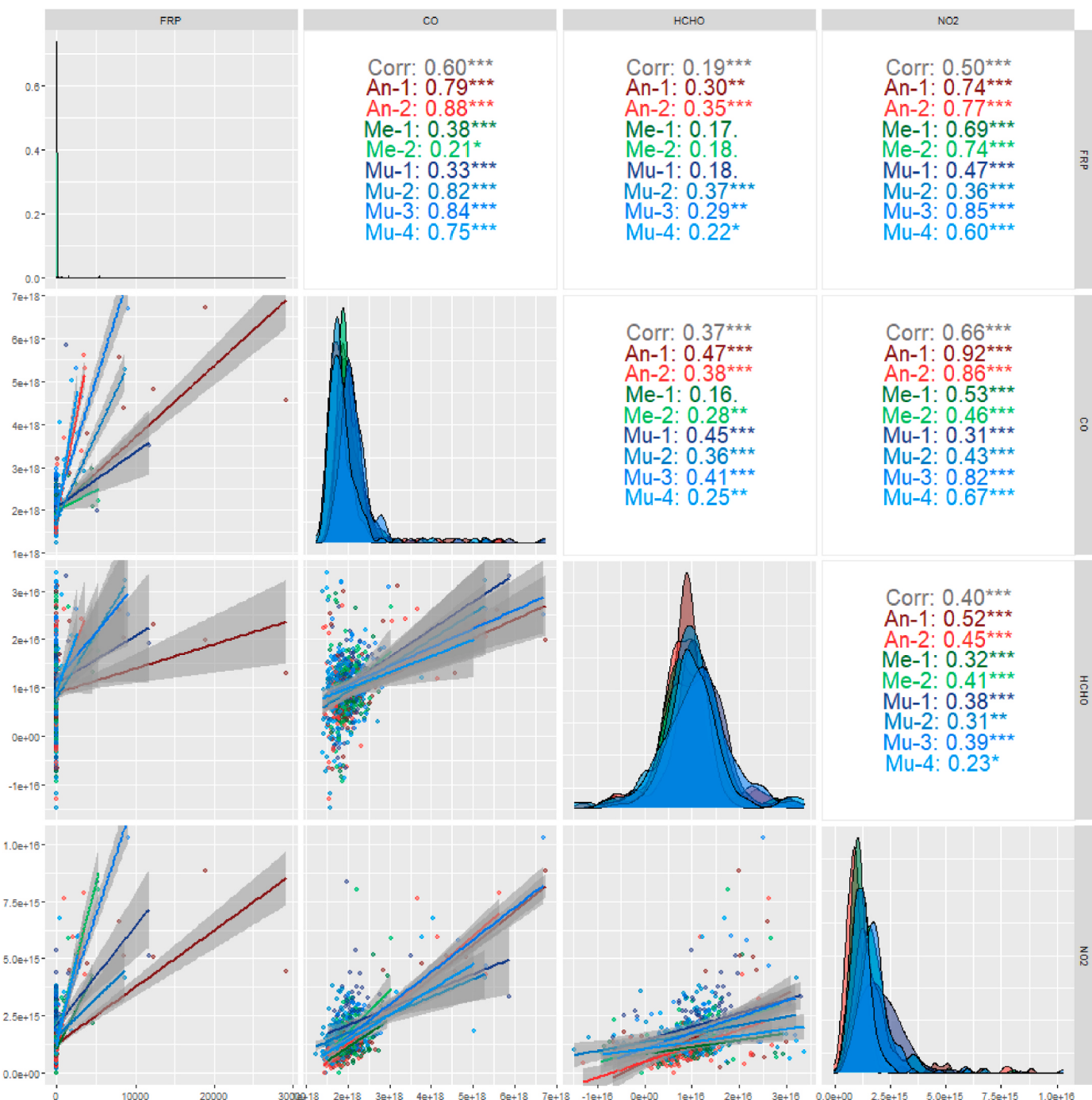


**Fig. 6.** Correlations between daily FRP, CO, HCHO, and NO<sub>2</sub> column concentrations for all FRs (p value of 0–0.001: \*\*\*, 0.001–0.01: \*\*, 0.01–0.05: \*).

indicated transport to south-southwest for Antalya, south-southwest for Mugla, and south-southeast for Mersin FRs. Maps of CO showed two maxima well offshore in the Mediterranean Sea, HCHO signals were more dispersed and closer to the FRs, and NO<sub>2</sub> indicated highest levels over FRs with a smaller area. Comparison of pre-fire, fire, and post-fire periods indicated that CO and NO<sub>2</sub> pollution levels increased during the fire, and post-fire periods compared with pre-fire interval.

Correlations of CO and NO<sub>2</sub> with FRP were stronger as primary pollutants. Additionally, CO and NO<sub>2</sub> showed a strong correlation with each other indicating wildfires as the same pollution source. HCHO correlations with FRP were low and maximum HCHO levels were observed not over the FRs, but in the transported plume.

Overall, the study showed that 2021 summer wildfires in Turkey

resulted in decrease in air quality with increased pollution levels not only during the fire episode, but also in the post-fire period according to FR and transported column concentrations.

#### Data accessibility

Data supporting this publication are available from these websites: <https://disc.gsfc.nasa.gov/>, [https://sim.csb.gov.tr/STN/STN\\_Report/StationDataDownloadNew](https://sim.csb.gov.tr/STN/STN_Report/StationDataDownloadNew), and <https://firms.modaps.eosdis.nasa.gov/country/>

## Financial support

The study did not receive financial support from any institution.

## CRediT authorship contribution statement

**Merve Eke:** Writing – original draft, Visualization, Formal analysis. **Fulya Cingiroglu:** Writing – review & editing, Visualization, Investigation, Formal analysis. **Burcak Kaynak:** Writing – review & editing, Visualization, Supervision, Resources, Methodology, Conceptualization.

## Declaration of competing interest

The authors declare that they have no known competing financial interests or personal relationships that could have appeared to influence the work reported in this paper.

## Data availability

Data will be made available on request.

## Acknowledgements

We thank NASA Goddard Earth Sciences Data and Information Services Center (GES-DISC) and NASA Fire Information for Resource Management System (FIRMS) for providing data as open sources.

## Appendix A. Supplementary data

Supplementary data to this article can be found online at <https://doi.org/10.1016/j.atmosenv.2024.120445>.

## References

- Aguilera, R., Corrington, T., Gershunov, A., Benmarhnia, T., 2021. Wildfire smoke impacts respiratory health more than fine particles from other sources: observational evidence from Southern California. *Nat. Commun.* 12 (1), 1493. <https://doi.org/10.1038/s41467-021-21708-0>.
- Alvarado, L.M., Richter, A., Vrekoussis, M., Hilboll, A., Kalisz Hedegaard, A.B., Schneising, O., Burrows, J.P., 2020. Unexpected long-range transport of glyoxal and formaldehyde observed from the Copernicus Sentinel-5 Precursor satellite during the 2018 Canadian wildfires. *Atmos. Chem. Phys.* 20 (4), 2057–2072.
- Aurell, J., Gullett, B., Holder, A., Kiros, F., Mitchell, W., Watts, A., Ottmar, R., 2021. Wildland fire emission sampling at Fishlake National Forest, Utah using an unmanned aircraft system. *Atmos. Environ.* 247, 118193.
- Bondur, V.G., Voronova, O.S., Cherepanova, E.V., Tsidilina, M.N., Zima, A.L., 2020. Spatiotemporal analysis of multi-year wildfires and emissions of trace gases and aerosols in Russia based on satellite data. *Izvestiya Atmos. Ocean. Phys.* 56, 1457–1469.
- CAMS, 2021. <https://atmosphere.copernicus.eu/wildfires-wreaked-havoc-2021-cams-tracked-their-impact>. (Accessed 21 May 2023).
- CDC, 2008. Monitoring health effects of wildfires using the biosense system - San Diego County, California, October 2007, 2008 Jul 11 MMWR Morb. Mortal. Wkly. Rep. 57 (27), 741–744. PMID: 18614992.
- Chen, G., Guo, Y., Yue, X., Tong, S., Gasparini, A., Bell, M.L., Armstrong, B., Schwartz, J., Jaakkola, J.J.K., Zanobetti, A., Lavigne, E., Nascimento Saldiva, P.H., Kan, H., Royé, D., Milojevic, A., Overcenco, A., Urban, A., Schneider, A., Entezari, A., Ana Maria Vicedo-Cabrera, A.M., Zeka, A., Tobias, A., Nunes, B., Ahmad, B., Forsberg, B., Pan, S.-C., Iniguez, C., Ameling, C., De la Cruz Valencia, C., Åström, C., Houthuijs, D., Dung, D.V., Samoli, E., Mayvaneh, F., Sera, F., Carrasco-Escobar, G., Lei, Y., Orru, H., Kim, H., Iulian-Horia Holobaca, Kysely, J., Teixeira, J.P., Madureira, J., Katsouyanni, K., Hurtado-Díaz, M., Maasikmets, M., Ragettli, M.S., Hashizume, M., Stafoggia, M., Pascal, M., Scortichini, M., de Sousa, M., Stagliorio Coelho, Z., Ortega, N.V., Rytty, N.R.I., Scovronick, N., Matus, P., Goodman, P., Garland, R.M., Abrutsky, R., Garcia, S.O., Rao, S., Fratianni, S., Dang, T.N., Colistro, V., Huber, V., Lee, W., Seposo, X., Honda, H., You, Y.L., Ye, T., Yu, W., Abramson, M.J., Samet, J.M., Li, S., 2021. Mortality risk attributable to wildfire-related PM<sub>2.5</sub> pollution: a global time series study in 749 locations. *Lancet Planet. Health* 5 (9), e579–e587. [https://doi.org/10.1016/S2542-5196\(21\)00200-X](https://doi.org/10.1016/S2542-5196(21)00200-X).
- Chow, F.K., Yu, K.A., Young, A., James, E., Grell, G.A., Csiszar, I., Tsidulko, M., Freitas, S., Pereira, G., Giglio, L., Friberg, M.D., Ahmadov, R., 2022. High-resolution smoke forecasting for the 2018 camp fire in California. *Bull. Am. Meteorol. Soc.* 103 (6), E1531–E1552. <https://doi.org/10.1175/BAMS-D-20-0329.1>.
- Cook, P.A., Savage, N.H., Turquety, S., Carver, G.D., O'Connor, F.M., Heckel, A., Stewart, D., Whalley, L.K., Parker, A.E., Schlager, H., Singh, H.B., Avery, M.A., Sachse, G.W., Brune, W., Richter, A., Burrows, J.P., Purvis, R., Lewis, A.C., Reeves, C., E., Monks, P.S., Levine, J.G., Pyle, J.A., 2007. Forest fire plumes over the North Atlantic: p-TOMCAT model simulations with aircraft and satellite measurements from the ITOP/ICARTT campaign. *J. Geophys. Res. Atmos.* 112 (D10) <https://doi.org/10.1029/2006JD007563>.
- Cortes-Ramirez, J., Michael, R.N., Knibbs, L.D., Bambrick, H., Haswell, M.R., Wraith, D., 2022. The association of wildfire air pollution with COVID-19 incidence in New South Wales, Australia. *Sci. Total Environ.* 809, 151158.
- Crutzen, P.J., Heidt, L.E., Krasnec, J.P., Pollock, W.H., Seiler, W., 1979. Biomass burning as a source of atmospheric gases CO, H<sub>2</sub>, N<sub>2</sub>O, NO, CH<sub>3</sub>Cl and COS. *Nature* 282, 253–256.
- De Smedt, I., Pinardi, G., Vigouroux, C., Compernolle, S., Bais, A., Benavent, N., Boersma, F., Chan, K.-L., Donner, S., Eichmann, K.-U., Hedelt, P., Hendrick, F., Irie, H., Kumar, V., Lambert, J.-C., Langerock, B., Lerot, C., Liu, C., Loyola, D., Piters, A., Richter, A., Rivera Cardenas, C., Romahn, F., Ryan, R.G., Sinha, V., Theys, N., Vlietinck, J., Wagner, T., Wang, T., Yu, H., Van Roozendael, M., 2021. Comparative assessment of TROPOMI and OMI formaldehyde observations and validation against MAX-DOAS network column measurements. *Atmos. Chem. Phys.* 21 (16), 12561–12593. <https://doi.org/10.5194/acp-21-12561-2021>.
- Di Virgilio, G., Evans, J.P., Blake, S.A., Armstrong, M., Dowdy, A.J., Sharples, J., McRae, R., 2019. Climate change increases the potential for extreme wildfires. *Geophys. Res. Lett.* 46 (14), 8517–8526.
- EPA, 2022. Health effects Attributed to wildfire smoke. <https://www.epa.gov/wildfire-smoke-course/health-effects-attributed-wildfire-smoke>. (Accessed 18 May 2023).
- Fadadu, R.P., Grimes, B., Jewell, N.P., Vargo, J., Young, A.T., Abuabara, K., Balmes, J.R., Wei, M.L., 2021. Association of wildfire air pollution and health care use for atopic dermatitis and itch. *JAMA Dermatology* 157 (6), 658–666. <https://doi.org/10.1001/jamadermatol.2021.0179>.
- FIRMS, 2022. <https://firms.modaps.eosdis.nasa.gov/country/>. (Accessed 11 December 2022).
- Fuller, R., Landrigan, P.J., Balakrishnan, K., Bathan, G., Bose-O'Reilly, S., Brauer, M., Caravanos, J., Chiles, T., Cohen, A., Corra, L., Cropper, M., Ferraro, G., Hanna, J., Hanrahan, D., Hu, H., Hunter, D., Janata, G., Kupka, R., Lanphear, B., Lichtveld, M., Martin, K., Mustapha, A., Sanchez-Triana, E., Sandilya, K., Schaefli, L., Shaw, J., Seddon, J., Suk, W., Téllez-Rojo, M.M., Yan, C., 2022. Pollution and health: a progress update. *Lancet Planet. Health*. [https://doi.org/10.1016/S2542-5196\(22\)00090-0](https://doi.org/10.1016/S2542-5196(22)00090-0).
- Ges DISC, 2023. <https://disc.gsfc.nasa.gov/>. (Accessed 21 May 2023).
- Global Forest Watch, 2021. <https://www.globalforestwatch.org/map/>. (Accessed 6 January 2023).
- Gong, X., Kaufflau, A., Nair, U., Jaffe, D.A., 2017. Quantifying O<sub>3</sub> impacts in urban areas due to wildfires using a generalized additive model. *Environ. Sci. Technol.* 51 (22), 13216–13223.
- Griffin, D., Zhao, X., McLinden, C.A., Boersma, F., Bourassa, A., Dammers, E., Degenstein, D., Eskes, H., Fehr, L., Fioletov, V., Hayden, K., Kharol, S.K., Li, S.M., Makar, P., Martin, R.V., Mihele, C., Mittermeier, R.L., Krotkov, N., Sneep, M., Lamsal, L.N., ter Linden, M., van Geffen, J., Vreekind, P., Wolde, M., 2019. High-resolution mapping of nitrogen dioxide with TROPOMI: first results and validation over the Canadian oil sands. *Geophys. Res. Lett.* 46 (2), 1049–1060. <https://doi.org/10.1029/2018GL081095>.
- Griffin, D., McLinden, C.A., Dammers, E., Adams, C., Stockwell, C., Warneke, C., Bourgeois, I., Peischl, J., Ryerson, T.B., Zarzana, K.J., Rowe, J.P., Volkamer, R., Knote, C., Kille, N., Koenig, T.K., Lee, C.F., Rollins, D., Rickly, P.S., Chen, J., Fehr, L., Bourassa, A., Degenstein, D., Hayden, K., Mihele, C., Wren, S.N., Liggio, J., Akingunola, A., Makar, P., 2021. Biomass burning nitrogen dioxide emissions derived from space with TROPOMI: methodology and validation. *Atmos. Meas. Tech.* 14, 7929–7957. <https://doi.org/10.5194/amt-14-7929-2021>.
- Holloway, T., Miller, D., Anenberg, S., Diao, M., Duncan, B., Fiore, A.M., Henze, D.V., Hess, J., Kinney, P.L., Liu, Y., Neu, J.L., O'Neill, S.M., Odman, M.T., Pierce, R.B., Russell, A.G., Tong, D., West, J.J., Zondlo, M.A., 2021. Satellite monitoring for air quality and health. *Annual Review of Biomedical Data Science* 4, 417–447. <https://doi.org/10.1146/annurev-biodatasci-110920-093120>.
- Iban, M.C., Sahin, E., 2022. Monitoring burn severity and air pollutants in wildfire events using remote sensing data: the case of Mersin wildfires in summer 2021. *Gümüşhane Üniversitesi Fen Bilimleri Dergisi* 12 (2), 487–497.
- Jaffe, D.A., Wigder, N.L., 2012. Ozone production from wildfires: a critical review. *Atmos. Environ.* 51, 1–10.
- Jaffe, D.A., Wigder, N., Downey, N., Pfister, G., Boynard, A., Reid, S.B., 2013. Impact of wildfires on ozone exceptional events in the western US. *Environ. Sci. Technol.* 47 (19), 11065–11072.
- Jin, X., Zhu, Q., Cohen, R.C., 2021. Direct estimates of biomass burning NO x emissions and lifetimes using daily observations from TROPOMI. *Atmos. Chem. Phys.* 21 (20), 15569–15587.
- Jin, X., Fiore, A.M., Cohen, R.C., 2023. Space-based observations of ozone precursors within California wildfire plumes and the impacts on ozone–NO<sub>x</sub>–VOC chemistry. *Environ. Sci. Technol.* 57 (39), 14648–14660. <https://doi.org/10.1021/acs.est.9b07785>.
- Jones, M.W., Smith, A., Betts, R., Canadell, J.G., Prentice, I.C., Le Quéré, C., 2020. Climate change increases the risk of wildfires. *Sci. Brief. Rev.* 116, 117.
- Justice, C.O., Román, M.O., Csiszar, I., Vermote, E.F., Wolfe, R.E., Hook, S.J., Friedl, M., Wang, Z., Schaaf, C.B., Miura, T., Tschudi, M., Riggs, G., Hall, D.K., Lyapustin, A.I., Devadiga, S., Davidson, C., Masuoka, E.J., 2013. Land and cryosphere products from Suomi NPP VIIRS: overview and status. *J. Geophys. Res. Atmos.* 118 (17), 9753–9765. <https://doi.org/10.1002/jgrd.50771>.
- Keeley, J.E., Syphard, A.D., 2021. Large California wildfires: 2020 fires in historical context. *Fire Ecology* 17 (1), 1–11.

- Langford, A.O., Senff, C.J., Alvarez II, R.J., Aikin, K.C., Ahmadov, R., Angevine, W.M., Baidar, S., Brewer, W.A., Brown, S.S., James, E.P., McCarty, B.J., Sandberg, S.P., Zucker, M.L., 2023. Were wildfires responsible for the unusually high surface ozone in Colorado during 2021? *J. Geophys. Res. Atmos.* 128 <https://doi.org/10.1029/2022JD037700Lee> e2022JD037700.
- Lee, J.D., Squires, F.A., Sherwen, T., Wilde, S.E., Cliff, S.J., Carpenter, L.J., Hopkins, J.R., Bauguitte, S.J., Reed, C., Barker, P., Allen, G., Bannan, T.J., Matthews, E., Mehra, A., Percival, C., Heard, D.E., Whalley, L.K., Ronnie, G.V., Seldon, S., Ingham, T., Keller, C.A., Knowland, K.E., Nisbet, E.G., Andrews, S., 2021. Ozone production and precursor emission from wildfires in Africa. *Environ. Sci. J. Integr. Environ. Res.: Atmosphere* 1 (7), 524–542.
- Li, Y., Mickley, L.J., Liu, P., Kaplan, J.O., 2020. Trends and spatial shifts in lightning fires and smoke concentrations in response to 21<sup>st</sup> century climate over the national forests and parks of the western United States. *Atmos. Chem. Phys.* 20 (14), 8827–8838.
- Liao, J., Wolfe, G.M., Hannun, R.A., St Clair, J.M., Hanisco, T.F., Gilman, J.B., Lamplugh, A., Selimovic, V., Diskin, G.S., Nowak, J.B., Halliday, H.S., DiGangi, J.P., Hall, S.R., Ullmann, K., Holmes, C.D., Fite, C.H., Agastra, A., Ryerson, T.B., Peischl, J., Bourgeois, I., Warneke, C., Coggon, M.M., Gkatzelis, G.I., Sekimoto, K., Fried, A., Richter, D., Weibring, P., Apel, E.C., Hornbrook, R.S., Brown, S.S., Womack, C.C., Robinson, M.A., Washenfelder, R.A., Veres, P.R., Neuman, J.A., 2021. Formaldehyde evolution in US wildfire plumes during the fire influence on regional to global environments and air quality experiment (FIREX-AQ). *Atmos. Chem. Phys.* 21 (24), 18319–18331. <https://doi.org/10.5194/acp-21-18319-2021>.
- Liú, J.C., Pereira, G., Uhl, S.A., Bravo, M.A., Bell, M.L., 2015. A systematic review of the physical health impacts from non-occupational exposure to wildfire smoke. *Environ. Res.* 136, 120–132. <https://doi.org/10.1016/j.envres.2014.10.015>.
- Matz, C.J., Egyed, M., Xi, G., Racine, J., Pavlovic, R., Rittmaster, R., Henderson, S.B., Stieb, D.M., 2020. Health impact analysis of PM<sub>2.5</sub> from wildfire smoke in Canada (2013–2015, 2017–2018). *Sci. Total Environ.* 725, 138506 <https://doi.org/10.1016/j.scitotenv.2020.138506>.
- McNeill, V.F., Thornton, J.A., 2023. How wildfires deplete ozone in the stratosphere. *Nature* 615, 219–221.
- Mickley, L.J., Jacob, D.J., Rind, D., 2001. Uncertainty in preindustrial abundance of tropospheric ozone: implications for radiative forcing calculations. *J. Geophys. Res. Atmos.* 106 (D4), 3389–3399.
- MoAF, 2020. Turkey's Forest Presence. <https://www.ogm.gov.tr/tr/ormanlarimiz/Turkiye-Orman-Varligi>. (Accessed 21 May 2023).
- MoEUCC, 2022. [https://sim.csb.gov.tr/STN/STN\\_Report/StationDataDownloadNew](https://sim.csb.gov.tr/STN/STN_Report/StationDataDownloadNew). (Accessed 21 May 2023).
- Naqvi, H.R., Mutreja, G., Shakeel, A., Singh, K., Abbas, K., Naqvi, D.F., Chaudhary, A.A., Siddiqui, M.A., Gautam, A.A., Gautam, S., Naqvi, A.R., 2023. Wildfire-induced pollution and its short-term impact on COVID-19 cases and mortality in California. *Gondwana Res.* 114, 30–39. <https://doi.org/10.1016/j.gr.2022.04.016>.
- Parente, J., Pereira, M.G., Amraoui, M., Fischer, E.M., 2018. Heat waves in Portugal: current regime, changes in future climate and impacts on extreme wildfires. *Sci. Total Environ.* 631, 534–549.
- Pechony, O., Shindell, D.T., 2010. Driving forces of global wildfires over the past millennium and the forthcoming century. *Proc. Natl. Acad. Sci. USA* 107 (45), 19167–19170.
- Peng, Q., Palm, B.B., Fredrickson, C.D., Lee, B.H., Hall, S.R., Ullmann, K., Campos, T., Weinheimer, A.J., Apel, E.C., Flocke, F., Permar, W., Hu, L., Garofalo, L.A., Pothier, M.A., Farmer, D.K., Ku, I.-T., Sullivan, A.P., Collett Jr., J.L., Fischer, E., Thornton, J.A., 2021. Observations and modeling of NO<sub>x</sub> photochemistry and fate in fresh wildfire plumes. *ACS Earth Space Chem.* 5 (10), 2652–2667. <https://doi.org/10.1021/acsearthspacechem.1c00086>.
- Pouyaei, A., Mizzi, A.P., Choi, Y., Mousavinezhad, S., Khorshidian, N., 2023. Downwind ozone changes of the 2019 wildfires flotsam: insights from WRF-chem/DART assimilation of OMI NO<sub>2</sub>, HCHO, and MODIS AOD retrievals. *J. Geophys. Res. Atmos.* 128, e2022JD038019 <https://doi.org/10.1029/2022JD038019>.
- Reid, C.E., Brauer, M., Johnston, F.H., Jerrett, M., Balmes, J.R., Elliott, C.T., 2016. Critical review of health impacts of wildfire smoke exposure. *Environ. Health Perspect.* 124 (9), 1334–1343.
- Requia, W.J., Amini, H., Mukherjee, R., Gold, D.R., Schwartz, J.D., 2021. Health impacts of wildfire-related air pollution in Brazil: a nationwide study of more than 2 million hospital admissions between 2008 and 2018. *Nat. Commun.* 12 (1), 6555.
- Richards, J., Husar, R., Bevacqua, E., Zscheischler, J., 2022. Insights into the Drivers and Spatio-Temporal Trends of Extreme Mediterranean Wildfires with Statistical Deep-Learning. *arXiv preprint arXiv:2212.01796*.
- Ryan, R.G., Silver, J.D., Schofield, R., 2021. Air quality and health impact of 2019–20 Black Summer megafires and COVID-19 lockdown in Melbourne and Sydney, Australia. *Environ. Pollut.* 274, 116498.
- Schneider, S.R., Lee, K., Santos, G., Abbatt, J.P., 2021. Air quality data approach for defining wildfire influence: impacts on PM<sub>2.5</sub>, NO<sub>2</sub>, CO, and O<sub>3</sub> in Western Canadian cities. *Environ. Sci. Technol.* 55 (20), 13709–13717.
- Schneising, O., Buchwitz, M., Reuter, M., Bovensmann, H., Burrows, J.P., 2020. Severe Californian wildfires in November 2018 observed from space: the carbon monoxide perspective. *Atmos. Chem. Phys.* 20 (6), 3317–3332.
- Sha, M.K., Langerock, B., Blavier, J.-F.L., Blumenstock, T., Borsdorff, T., Buschmann, M., Dehn, A., De Maziere, M., Deutscher, N.M., Feist, D.G., Garcia, O.E., Griffith, D.W.T., Grutter, M., Hannigan, J.W., Hase, F., Heikkinen, P., Hermans, C., Iraci, L.T., Jeseck, P., Jones, N., Kivi, R., Kumps, N.L., graf, J., Lorente, A., Mahieu, E., Makarova, M.V., Mellqvist, J., Metzger, J.-M., Morino, I., Nagahama, T., Notholt, J., Ohyama, H., Ortega, I., Palm, M., Petri, C., Pollard, D.F., Rettinger, M., Robinson, J., Roche, S., Roehl, C.M., Rohling, A.N., Rousogenous, C., Schneider, M., Shiomi, K., Smale, D., Stremme, W., Strong, K., Sussmann, R., Te, Y., Uchino, O., Velasco, V.A., Vigouroux, C., Vrekoussis, M., Wang, P., Warneke, T., Wizenberg, T., Wunch, D., Yamanouchi, S., Yang, Y., Zhou, M., 2021. Validation of methane and carbon monoxide from Sentinel-5 Precursor using TCCON and NDACC-IRWG stations. *Atmos. Meas. Tech.* 14 (9), 6249–6304. <https://doi.org/10.5194/amt-14-6249-2021>.
- Shi, G., Yan, H., Zhang, W., Dodson, J., Heijnis, H., Burrows, M., 2021. Rapid warming has resulted in more wildfires in northeastern Australia. *Sci. Total Environ.* 771, 144888.
- Sillman, S., Logan, J.A., Wofsy, S.C., 1990. The sensitivity of ozone to nitrogen oxides and hydrocarbons in regional ozone episodes. *J. Geophys. Res. Atmos.* 95 (D2), 1837–1851.
- Tao, Z., He, H., Sun, C., Tong, D., Liang, X.Z., 2020. Impact of fire emissions on US air quality from 1997 to 2016—A modeling study in the satellite era. *Rem. Sens.* 12 (6), 913.
- Tarfín-Carrasco, P., Augusto, S., Palacios-Peña, L., Ratola, N., Jiménez-Guerrero, P., 2021. Impact of large wildfires on PM 10 levels and human mortality in Portugal. *Nat. Hazards Earth Syst. Sci.* 21 (9), 2867–2880.
- Tariq, S., ul-Haq, Z., Mariam, A., Mahmood, U., Ahmed, W., 2022. Assessment of air quality during worst wildfires in Mugla and Antalya regions of Turkey. *Nat. Hazards* 1–20.
- Theys, N., Volkamer, R., Müller, J.F., Zarzana, K.J., Kille, N., Clarisse, L., De Smedt, I., Lerot, C., Hendrick, F., Koenig, T.K., Lee, C.F., Yu, H., Van Roozendael, M., 2020. Global nitrous acid emissions and levels of regional oxidants enhanced by wildfires. *Nat. Geosci.* 13 (10), 681–686. <https://doi.org/10.1038/s41561-020-0637-7>.
- TROPOMI, 2023. TROPOMI Mission Status. <https://www.tropomi.eu/mission-status>. (Accessed 21 May 2023).
- TSMS, 2022. <https://mevbis.mgm.gov.tr/mevbis/ui/index.html#/Workspace>. (Accessed 12 December 2022).
- Turco, M., Llasat, M.C., von Hardenberg, J., Provenzale, A., 2014. Climate change impacts on wildfires in a Mediterranean environment. *Climatic Change* 125 (3–4), 369–380.
- Urbanski, S.P., Hao, W.M., Baker, S., 2008. Chemical composition of wildland fire emissions. *Dev. Environ. Sci.* 8, 79–107.
- van Geffen, J., Boersma, K.F., Eskes, H., Sneep, M., ter Linden, M., Zara, M., Veefkind, J.P., 2020. SSP TROPOMI NO<sub>2</sub> slant column retrieval: method, stability, uncertainties and comparisons with OMI. *Atmos. Meas. Tech.* 13, 1315–1335. <https://doi.org/10.5194/amt-13-1315-2020>.
- Veefkind, J.P., Aben, I., McMullan, K., Förster, H., Vries, J.D., Otter, G., Claas, J., Eskes, H.J., de Haan, J.F., Kleipool, Q., van Weele, M., Hasekamp, O., Hoogeveen, R., Landgraf, J., Snel, R., Tol, P., Ingmann, P., Voors, R., Kruizinga, B., Vink, R., Visser, H., Levelt, P.F., 2012. TROPOMI on the ESA Sentinel-5 Precursor: a GMES mission for global observations of the atmospheric composition for climate, air quality and ozone layer applications. *Rem. Sens. Environ.* 120, 70–83. <https://doi.org/10.1016/j.rse.2011.09.027>.
- Vigouroux, C., Langerock, B., Bauer-Aquino, C.A., Blumenstock, T., Cheng, Z., De Maziere, M., De Smedt, I., Grutter, M., Hannigan, J.W., Jones, N., Kivi, R., Loyola, D., Lutsch, E., Mahieu, E., Makarova, M., Metzger, J.M., Morino, I., Murata, I., Nagahama, T., Notholt, J., Ortega, I., Palm, M., Pinardi, G., Röhling, A., Smale, D., Stremme, W., Strong, K., Sussmann, S., Té, Y., van Roozendael, M., Wang, P., Winkler, H., 2020. TROPOMI–Sentinel-5 Precursor formaldehyde validation using an extensive network of ground-based Fourier-transform infrared stations. *Atmos. Meas. Tech.* 13 (7), 3751–3767. <https://doi.org/10.5194/amt-13-3751-2020>.
- Wang, P., Holloway, T., Bindl, M., Harkey, M., De Smedt, I., 2022. Ambient formaldehyde over the United States from ground-based (AQS) and satellite (OMI) observations. *Rem. Sens.* 14 (9), 2191.
- Xue, Z., Gupta, P., Christopher, S., 2021. Satellite-based estimation of the impacts of summertime wildfires on PM<sub>2.5</sub> concentration in the United States. *Atmos. Chem. Phys.* 21 (14), 11243–11256. <https://doi.org/10.5194/acp-21-11243-2021>.
- Yin, L., Du, P., Zhang, M., Liu, M., Xu, T., Song, Y., 2019. Estimation of emissions from biomass burning in China (2003–2017) based on MODIS fire radiative energy data. *Biogeosciences* 16 (7), 1629–1640. <https://doi.org/10.5194/bg-16-1629-2019>.
- Yin, S., Wang, X., Guo, M., Santoso, H., Guan, H., 2020. The abnormal change of air quality and air pollutants induced by the forest fire in Sumatra and Borneo in 2015. *Atmos. Res.* 243, 105027.
- Zhao, T., Mao, J., Simpson, W.R., De Smedt, I., Zhu, L., Hanisco, T.F., Wolfe, G.M., St Clair, J.M., Abad, G.G., Nowlan, C.R., Barletta, B., Meinardi, S., Blake, D.R., Apel, E.C., Hornbrook, R.S., 2022. Source and variability of formaldehyde (HCHO) at northern high latitudes: an integrated satellite, aircraft, and model study. *Atmos. Chem. Phys.* 22 (11), 7163–7178. <https://doi.org/10.5194/acp-22-7163-2022>.